ACS APPLIED MATERIALS & INTERFACES

RESEARCH ARTICLE

www.acsami.org

Enhancing the Oxygen Permeability of $BaCo_{0.7}Fe_{0.2}Nb_{0.1}O_{3-\delta}$ Membranes by Coating $GdBaCo_{2-x}Fe_xO_{5+\delta}$ for Partial Oxidation of Coke Oven Gas to Syngas

Hongwei Cheng,* Jizhong Liu, Xionggang Lu,* and Weizhong Ding

Shanghai Key Laboratory of Modern Metallurgy and Materials Processing, Shanghai University, Number 275 Mailbox, 149 Yanchang Road, Shanghai 200072, People's Republic of China

ABSTRACT: The dense ceramic membranes $BaCo_{0.7}Fe_{0.2}Nb_{0.1}O_{3-\delta}$ (BCFN) combined with $GdBaCo_{2-x}Fe_xO_{5+\delta}$ ($0 \le x \le 2.0$) surface modification layers was investigated for hydrogen production by partial oxidation reforming of coke oven gas (COG). As oxygen permeation of BCFN membrane is controlled by the rate surface exchange kinetics, the $GdBaCo_{2-x}Fe_xO_{5+\delta}$ materials improve the oxygen permeation flux of the BCFN membrane by 20−44% under helium atmosphere at 750 °C. The maximum oxygen permeation flux reached 14.4 mL min^{-1} cm^{-2} in the $GdBaCoFeO_{5+\delta}$ coated BCFN membrane reactor at 850 °C, and a CH_4 conversion of 94.9%, a H_2 selectivity of 88.9%, and a CO selectivity of 99.6% have been achieved. The $GdBaCo_{2-x}Fe_xO_{5+\delta}$ coating materials possess uniform porous structure, fast oxygen desorption rate and good compatibility with the membrane, which showed a potential application for the surface modification of the membrane reactor.

KEYWORDS: hydrogen production, oxygen-permeation membrane, surface-coating, coke oven gas, partial oxidation

1. INTRODUCTION

Hydrogen is regarded as the most promising energy carrier in the 21st century owing to its highly efficient, nonpolluting and abundant sources characters.[1−3] Tremendous efforts are being undertaken to explore high-efficiency and large-scale technologies for hydrogen production. At present, hydrogen can be produced from a wide range of source materials including hydrocarbons, alcohol, biomass, and some industrial chemical byproducts.[4−6] Among them, coke oven gas (COG) is gaining increasing attention as one of the most attractive sources for low-cost hydrogen production.[7,8] Especially in China, the coke tonnage of above 388 million tons ranks as the first in the world and the corresponding amount of COG has reached 163 billion Nm^3 in 2010. The main components of COG are 54−59% hydrogen and 24−28% methane. Theoretically, by high-temperature desulfurization, reforming and water-gas shift reaction, the amount of hydrogen produced is more than that of original hydrogen in the COG. Of these cases, catalytic partial oxidation of CH_4 in COG using a ceramic oxygen-permeable membrane reactor is considered as an efficient and low-cost method to produce hydrogen.[9−13] This technology could significantly reduce the energy and the cost for hydrogen production by eliminating the need for an individual oxygen production plant.

During the past several years, ceramic membranes with mixed oxygen ionic and electronic conducting (MIEC) properties have been exploited deeply in the fields of oxygen separation and partial oxidation of methane to syngas.[14−16] One of the key targets for the development of membrane reactor is improving its oxygen-permeation rate and structural stability under reductive environment. It is well-known that the oxygen transport in a membrane is limited mainly by oxygen-ion diffusion in the membrane bulk and oxygen exchange on the surfaces of the membrane. The oxygen permeation flux in a dense ceramic membrane can be increased by reducing the thickness of the membrane until it is less than L_c, where the L_c is the critical membrane thickness, which determines the transition from bulk-diffusion limit to surface-exchange kinetics limit for the permeation. If the thickness of membrane is smaller than L_c, the oxygen surface exchange rate will become a dominant factor. In our previous work, the result have been confirmed that the rate-determining steps of the oxygen permeation in $BaCo_{0.7}Fe_{0.2}Nb_{0.1}O_{3-\delta}$ (BCFN) membrane with a thickness of about 1.0 mm are both the oxygen exchange on the surface and the bulk diffusion.[17] In fact, for practical applications, disk-shaped or tubular membrane reactors should have a relative reasonable mechanical strength, and the thickness of the membranes is always near to or over 1.0 mm. Therefore, any further increase in the permeation rate can be achieved only by coating a catalytic thin layer on the surface of the membrane. First, the coating layer should have a porous structure, the higher surface/volume ratios can enhance the ability of oxygen surface exchange kinetics. Second, the materials should present a faster oxygen surface exchange rate (desorption, dissociation, and oxidation) than the membrane.

Recent efforts to increase the oxygen flux have been heavily addressed by several groups. The enhancement of oxygen permeation flux was reached successfully by simple roughening leading to bigger effective surface area and higher surface/volume ratios.[18] The application of the perovskite-related oxide $GdBaCo_2O_{5+\delta}$ porous layer into dense $Ba_{0.5}Sr_{0.5}Co_{0.8}Fe_{0.2}O_{3-\delta}$ membrane have boosted its oxygen permeation flux greatly.[19] Furthermore, the deposition of the porous layer of $Ba_{0.5}Sr_{0.5}Co_{0.8}Fe_{0.2}O_{3-\delta}$ into a new cobalt-free $BaCe_{0.15}Fe_{0.85}O_{3-\delta}$ membrane also resulted in increased oxygen permeation flux.[20] Other options include the

Received: July 7, 2011
Accepted: September 19, 2011
Published: September 19, 2011

dx.doi.org/10.1021/am200892b | *ACS Appl. Mater. Interfaces* 2011, 3, 4032–4039

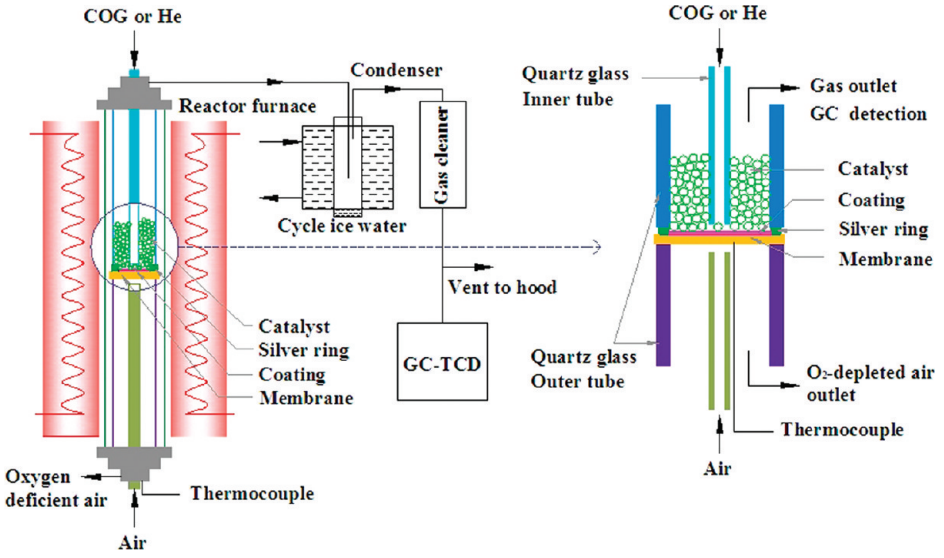

Figure 1. Schematic diagram of the membrane reactor system and gas flow direction.

use of the porous coating material with a high surface area and subsequently modifying the porous surface by impregnation with catalytically active metals, e.g., Pt, Ag, or Pr oxide.[21,22] A smart breakthrough idea is to use the porous coating layered with the membrane made from the same material to get rid the compatibility problem. Chen et al.[23] proposed a new configuration of $Ba_{0.5}Sr_{0.5}Co_{0.8}Fe_{0.2}O_{3-\delta}$ membrane with layered $Ba_{0.5}Sr_{0.5}Co_{0.2}Fe_{0.8}O_{3-\delta}$ as the thin-film and showed that the oxygen permeation flux was about 3.5 times higher than that of the $Ba_{0.5}Sr_{0.5}Co_{0.2}Fe_{0.8}O_{3-\delta}$ membrane under the same conditions. Recently, our research group has applied disk-type BCFN membrane by solid state reaction to the partial oxidation of COG for hydrogen production.[9−13,17] It was reported that the oxygen permeation flux and structural stability of the BCFN membranes coated by a $Ce_{0.8}Re_{0.2}O_{2-\delta}$ (Re = Sm, Gd) surface modification layers showed significant enhancement.

Among the various coating materials, the $LnBaCo_2O_{5+\delta}$ perovskite-related oxides has drawn extensive attention in recent years due to the wide variations in oxygen contents ($5+\delta$) and their promising MIEC properties.[24−26] A great deal of experimental effort has been made toward the study of $LnBaCo_2O_{5+\delta}$, in which Ln is a trivalent rare earth. However, The replacement of one transition-metal ion by another one could have a great impact on their MIEC properties.[27,28] In view of this, the purpose of the present work was to use the double perovskite oxides $GdBaCo_{2-x}Fe_xO_{5+\delta}$ as a coating layer on the BCFN membrane hopefully to improve oxygen permeability of the membrane and to find the most desirable materials which can act as effective catalytic coating layers on dense ceramic membranes. The effects of Fe substitution for Co in $GdBaCo_{2-x}Fe_xO_{5+\delta}$ coating layers, reaction temperature, air and He sweep flow rates on oxygen permeation fluxes of the membrane reactors were also examined.

2. EXPERIMENTAL SECTION

2.1. Materials Preparation. The $Ni/Ce_{0.75}Zr_{0.25}O_2/Mg_3(Al)O$ catalyst was prepared by the same method as that described in our previous work.[17] The $BaCo_{0.7}Fe_{0.2}Nb_{0.1}O_{3-\delta}$ (BCFN) membrane was prepared by conventional solid-state reaction methods. A stoichiometric mixture of $BaCO_3$, Co_3O_4, Fe_2O_3, and Nb_2O_5 powders was ball milled in ethanol using zirconia grinding media for 72 h, then dried overnight and calcined at 950 °C for 20 h with heating and cooling rates of 2−3 °C min^{-1}. The calcined powder was ball milled in ethanol for a further 72 h, and then dried overnight at 110 °C. Subsequently, the oxide powder was pressed into disk-shaped pellets using a stainless steel mold (20.0 mm diameter) under approximately 1.2×10^8 Pa hydraulic pressure, and finally sintered at 1110 °C in ambient air for 8 h with heating and cooling rates of 1−2 °C min^{-1}. The final diameter and thickness of the membranes were about 16.5 and 1.5 mm, respectively.

$GdBaCo_{2-x}Fe_xO_{5+\delta}$ (x = 0, 0.5, 1.0, 1.5, 2.0) composite oxides coating materials were synthesized via combined EDTA-citrate complexing sol−gel method. The necessary amount of Gd_2O_3 was first dissolved in HNO_3 solution under heating and stirring, then the calculated amounts of $Ba(NO_3)_2$, $Co(NO_3)_2 \cdot 6H_2O$, and $Fe(NO_3)_3 \cdot 9H_2O$ were added to the solution. After stirring for certain time, proper amounts of EDTA and citric acid were introduced, which served as the complexing agents. The mole ratio of total metal ions: EDTA: citric acid in the solution was controlled to be 1:1:2, and the pH value was adjusted to around 6 with $NH_3 \cdot H_2O$. Subsequently, the solution was heated continuously at 90 °C until sufficient water had evaporated that a dark purple gel was obtained. This gel was then dried overnight at 110 °C and prefired at 300 °C for several hours, then finally calcinated at 950 °C for 2 h under an air atmosphere to obtain the powder with final composition. The $GdBaCo_{2-x}Fe_xO_{5+\delta}$-coated ($x$ = 0, 0.5, 1.0, 1.5, 2.0) BCFN membranes (named BCFN-x) were prepared with spin-coating method. The coating paste was a mixture of 9 wt % $GdBaCo_{2-x}Fe_xO_{5+\delta}$ powder, 90 wt % terpineol, 0.2 wt % of carbon fiber, 0.3 wt % glycol, and 0.5 wt % ethyl cellulose. The $GdBaCo_{2-x}Fe_xO_{5+\delta}$ layer was coated on the permeation side of the BCFN membrane. Postheat treatment was conducted to remove the organic additives at 950 °C for 2 h with heating and cooling rates 2 °C min^{-1}.

2.2. Sample Characterization. X-ray diffraction (XRD, Rigaku D/Max-2550) was used to characterize the phase evolution of the coating materials and membranes.

The changes of the morphology of the coating materials and membranes were observed using a scanning electron microscope (SEM, JEOL JSM-6700F).

Thermogravimetric analyzer (TGA, Thermo Cahn TherMax 700) was used to detect the oxygen adsorption and desorption rate properties of the coating layer materials and BCFN. About 0.5 g of the sample was loaded into an alumina pan and heated to 850 °C under a 20 mol % O_2/He

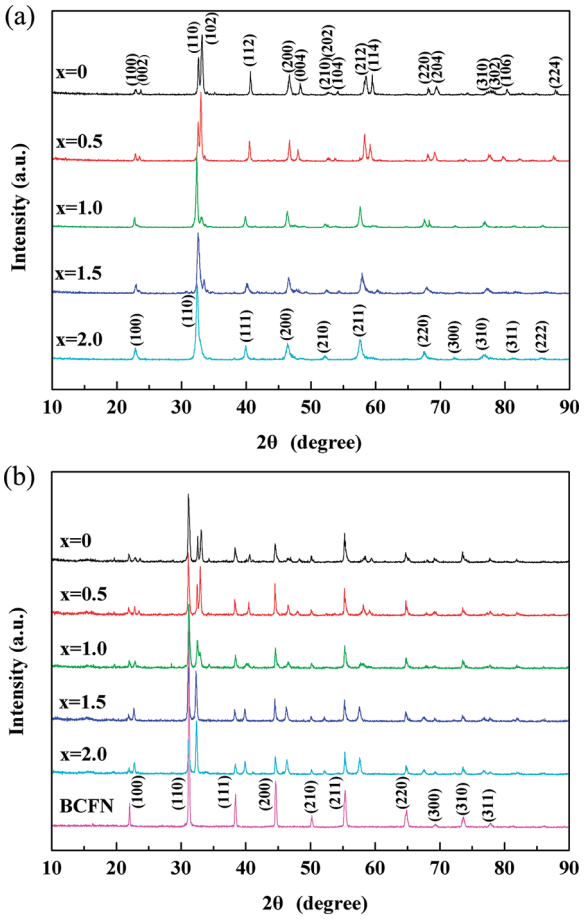

Figure 2. XRD patterns of the samples: (a) the $GdBaCo_{2-x}Fe_xO_{5+\delta}$ calcined at 950 °C for 2 h; (b) the BCFN membrane and the $GdBaCo_{2-x}Fe_xO_{5+\delta}$-coated BCFN membranes calcined at 950 °C for 2 h.

atmosphere. When the weight of the sample did not change any more, 20 mol % O_2/He was exchanged with He quickly. Then He was exchanged with 20 mol % O_2/He again when the weight did not decrease remarkably. The flow rate of the 20 mol % O_2/He and He was 100 mL min^{-1}.

2.3. Experimental Setup. The schematic diagram of the partial oxidation of COG in BCFN membrane reactor combined with a surface-coating layer and the gas flowchart were presented in Figure 1. The gas flow rates were controlled by mass flow controllers. One side of the membrane was exposed to compressed air and the other side to He or COG (57.42% H_2, 32.00% CH_4, 7.47% CO, and 3.11% CO_2). On the permeation side of the membrane, H_2, CH_4, CO and CO_2 in the outlet gas, in which the water was removed by $Mg(ClO_4)_2$, were analyzed by a Varian CP 3800 gas chromatography (GC) with a thermal conductivity detector (TCD).

Prior to the start of a test, the ceramic disk membrane was polished to 1.0 mm thickness by 800-mesh abrasive paper, and sealed into the reactor with a silver seal. Gas-tightness of membrane was ensured by monitoring nitrogen and no nitrogen leakage was detected. The effective inner surface area of the membrane was controlled around 1.3 cm^2. A total of 1.0 g of 20−40 mesh the catalyst was directly placed on the membrane. A K-type thermocouple was placed at the center of the bed to monitor the reaction temperature. The oxygen permeability of the discoid sample was determined from the content of CO and CO_2 in the reacted gas, and the amount of H_2O was evaluated from the balance of hydrogen before and after the reaction. The flow rate of outlet gas was measured by a soap-membrane flow meter. The conversion of CH_4, the selectivity of H_2, CO, CO_2 and H_2O were defined as follows

$$CH_4 \text{ conversion}, \% = \frac{F^{in}_{CH_4} - F^{out}_{CH_4}}{F^{in}_{CH_4}} \times 100;$$

$$H_2 \text{ selectivity}, \% = \frac{F^{out}_{H_2} - F^{in}_{H_2}}{2(F^{in}_{CH_4} - F^{out}_{CH_4})} \times 100$$

$$CO \text{ selectivity}, \% = \frac{F^{out}_{CO} - F^{in}_{CO}}{F^{in}_{CH_4} - F^{out}_{CH_4}} \times 100;$$

$$CO_2 \text{ selectivity}, \% = \frac{F^{out}_{CO_2} - F^{in}_{CO_2}}{F^{in}_{CH_4} - F^{out}_{CH_4}} \times 100$$

$$H_2O \text{ selectivity}, \% = \frac{2F^{in}_{CH_4} + F^{in}_{H_2} - F^{out}_{H_2} - 2F^{out}_{CH_4}}{2(F^{in}_{CH_4} - F^{out}_{CH_4})} \times 100$$

where F^{in}_i and F^{out}_i were the flow rates of the inlet and outlet gas i, respectively.

3. RESULTS AND DISCUSSION

3.1. Characterization of Materials. Figure 2a depicts the room temperature XRD patterns of the $GdBaCo_{2-x}Fe_xO_{5+\delta}$ ($0 \le x \le 2.0$) samples after sintering at 950 °C for 2 h in Air. For $0 \le x \le 0.5$, the XRD patterns of the $GdBaCo_{2-x}Fe_xO_{5+\delta}$ compositions were identified as single-phase double-perovskites and indexed on the basis of a tetragonal structure.[29,30] However, the crystal structure changes from tetragonal to cubic, suggesting a lack of long-range ordering in the perovskite lattice with increasing Fe content ($x = 2.0$). Furthermore, it can be seen that the main XRD peaks of the $GdBaCo_{2-x}Fe_xO_{5+\delta}$ samples shift gradually toward the low-angle direction with increasing Fe content. This indicates that the lattice expansion increases with increase in doping content of larger ion-radius Fe^{3+} in cobalt-sites. The XRD patterns of the BCFN membrane and $GdBaCo_{2-x}Fe_xO_{5+\delta}$-coated BCFN membranes are presented in Figure 2b. According to the XRD patterns, there are not undesired solid state reactions between $GdBaCo_{2-x}Fe_xO_{5+\delta}$ and BCFN for the mixture sintered at 950 °C for 2 h. It indicates that $GdBaCo_{2-x}Fe_xO_{5+\delta}$ have a good chemical compatibility with BCFN below 950 °C.

The SEM micrographs of the coated membranes are shown in Figure 3. From Figures 3a−e, it can be seen that the cross-section images of the BCFN-x membranes possess the similar structure and geometry properties. Additionally, we can distinguish the porous layers, which had approximately 15 μm thickness, from the dense BCFN membrane. As seen in Figure 3f, the surface of the $GdBaCoFeO_{5+\delta}$ layer was porous due to the volatilization of organic solution during the postheat treatment. This porosity would provide adequate diffusion pathway near the surface and increase the effective surface area of the BCFN-1.0 membrane. All the other $GdBaCo_{2-x}Fe_xO_{5+\delta}$-coated BCFN membranes showed similar particle size distribution and morphology. In summary, it can be suggested that a sintering temperature of 950 °C provides good balance between the conflicting coating requirements of maintaining a porous, high surface-area structure while at the same time providing a strong, well-sintered and adherent layer.

Figure 4a compares the TG plots of the BCFN and $GdBaCo_{2-x}Fe_xO_{5+\delta}$ samples recorded in 20 mol % O_2/He with the temperature increasing from 100 to 850 °C. All the samples experience weight loss above about 250 °C due to the loss of

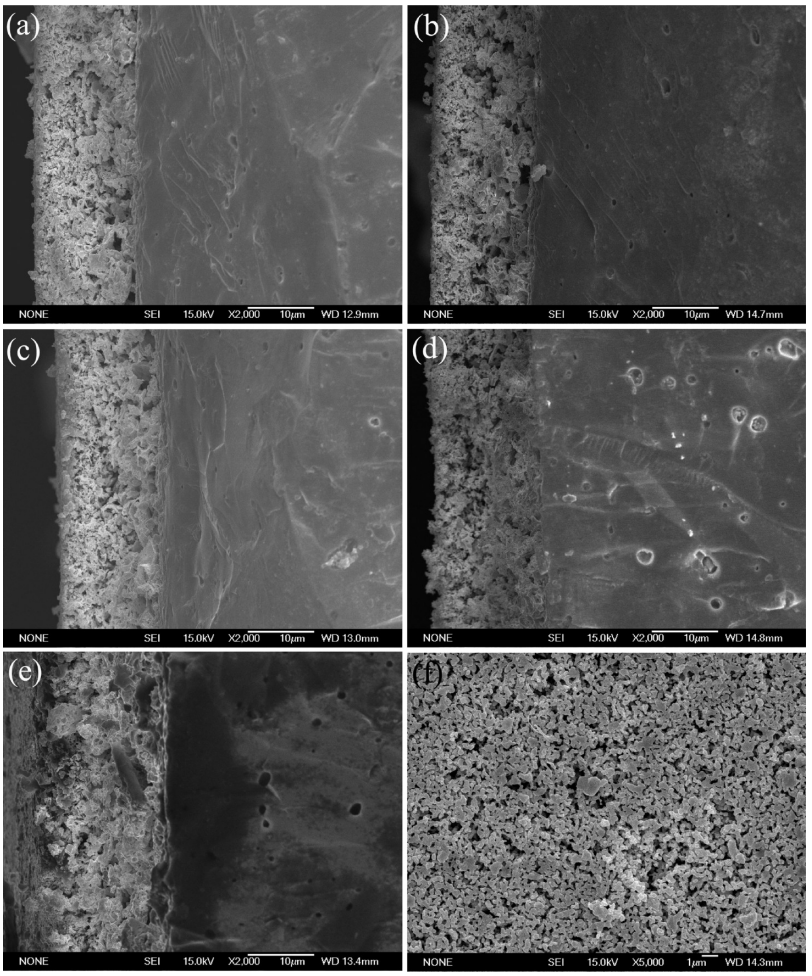

Figure 3. SEM images of the cross-section and surface of the fresh $GdBaCo_{2-x}Fe_xO_{5+\delta}$-coated BCFN membranes: (a) BCFN-0; (b) BCFN-0.5; (c, f) BCFN-1.0; (d) BCFN-1.5; (e) BCFN-2.0.

oxygen from the lattice, except for the BCFN sample that shows a slight initial weight gain before losing oxygen. This is because of the incomplete oxygen absorption during the cooling of the BCFN sample in the furnace following the synthesis firing at 1110 °C. A remarkable feature of $GdBaCo_{2-x}Fe_xO_{5+\delta}$ compounds is that all samples release more oxygen than BCFN at a certain temperature. Furthermore, it can be seen that the amount of oxygen released of $GdBaCo_2O_{5+\delta}$ and $GdBaCoFeO_{5+\delta}$ samples is several times than that in BCFN.

Figure 4b shows the weight change with the time during the gas changing cycle (20 mol % O_2/He→He→20 mol % O_2/He) at 850 °C. It can be seen that the weight of all the compounds will decrease (releasing oxygen) when gas flow is changed from O_2/He to He and increase (absorbing oxygen) when gas flow is changed from He to O_2/He. All of the samples show a slow weight loss in the oxygen desorption period and a rapid weight gain in the oxygen absorption period. However, the oxygen desorption rate of $GdBaCoFeO_{5+\delta}$ in He gas flow is faster than other samples at the same time points. Another thing needs to note is that the weight difference in O_2/He and He gas obtained in the transient TG experiment is smaller than that obtained in the temperature rising process (Figure 4a). One reason caused this difference may be that the time of oxygen desorption is not long enough for the sample to reach equilibrium with He in the transient TG experiment.

3.2. Oxygen Permeation of the Membranes. Figure 5 presents the influence of different coatings on the oxygen permeation flux through the membranes under the He atmosphere at 750−925 °C. It can be clearly seen that the addition of porous catalytic materials $GdBaCo_{2-x}Fe_xO_{5+\delta}$ on the membrane surface can sharply improve the oxygen permeation flux. We proposed that the rate-determining steps of the oxygen permeation in the BCFN membrane with 1.0 mm thickness are both the oxygen exchange on the surface and the bulk diffusion.[17] The enhancement of the oxygen permeation flux was mainly caused by the modification of oxygen potential drops at gas-membrane interfaces or the potential slope in the membrane due to the improvement of oxygen exchange rates by the porous layers.[31,32] The oxygen permeation flux through uncoated BCFN membrane was 0.86 mL min^{-1} cm^{-2} at 750 °C, whereas the value through the membrane coated using $GdBaCo_2O_{5+\delta}$ was 1.24 mL min^{-1} cm^{-2}, which was significantly 44% higher than that of uncoated BCFN membrane. Simultaneously, it can be noticed that the performance of the membrane reactors were greatly affected by the operating temperature. For instance, when the reaction temperature increased from 750 to 925 °C, the change of the experimental condition resulting from the oxygen permeation flux of the BCFN-$GdBaCoFeO_{5+\delta}$ membrane enhanced gradually from 1.20 to 2.16 mL min^{-1} cm^{-2}.

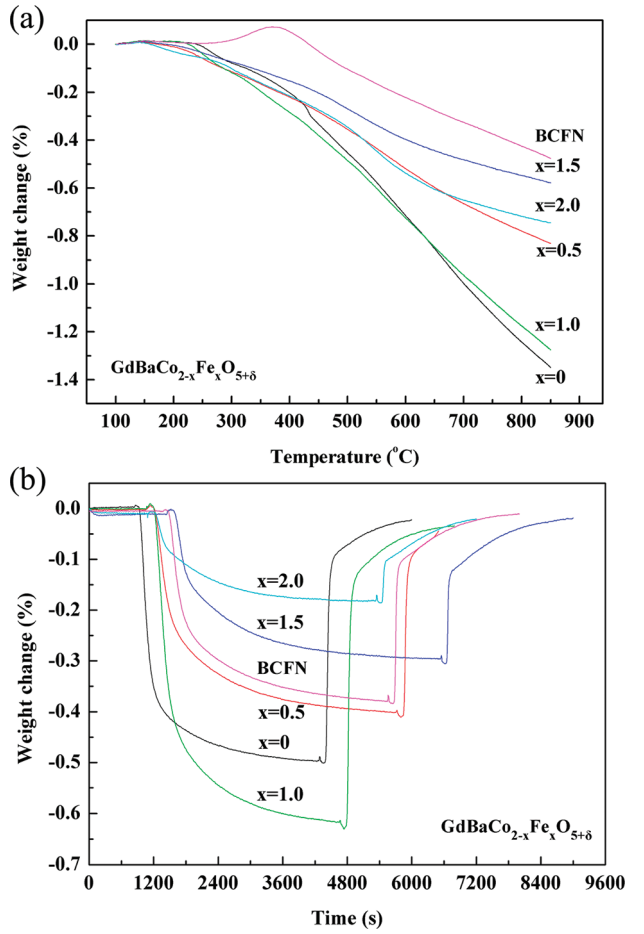

Figure 4. Weight change of the BCFN and $GdBaCo_{2-x}Fe_xO_{5+\delta}$ samples: (a) 20 mol % O_2/He atmosphere with the temperature increasing from 100 to 850 °C; (b) 20 mol % O_2/He → He → 20 mol % O_2/He cycle at 850 °C.

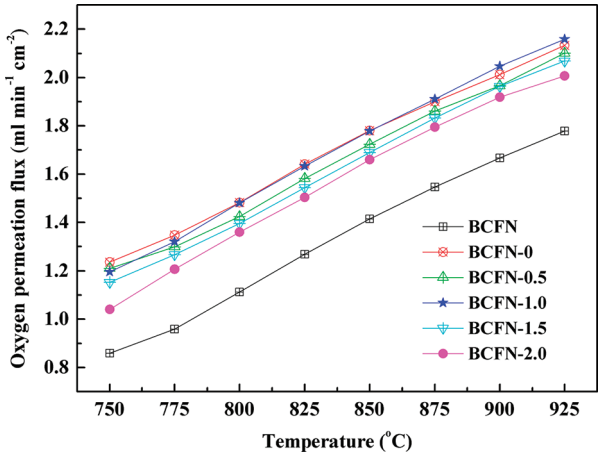

Figure 5. Effect of coatings and reaction temperature on oxygen permeation fluxes through the $GdBaCo_{2-x}Fe_xO_{5+\delta}$-coated BCFN membranes with 1.0 mm thickness. Reaction conditions: He flow rate, 100 mL min^{-1}; air flow rate, 200 mL min^{-1}.

Figure 6 shows the influence of the air flow rate on the oxygen permeation flux at 875 ∘C with a constant He flow rate of 100 mL min^{-1}. As shown in Figure 6, at the beginning the oxygen

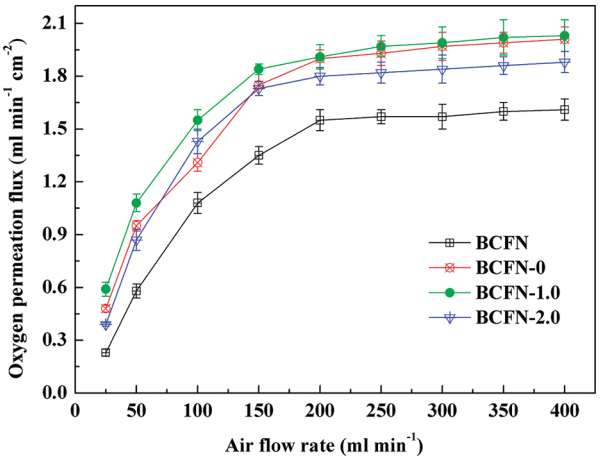

Figure 6. Effect of the air flow rate on oxygen permeation fluxes through the $GdBaCo_{2-x}Fe_xO_{5+\delta}$-coated BCFN membranes with 1.0 mm thickness. Reaction conditions: He flow rate, 100 mL min^{-1}; 875 °C.

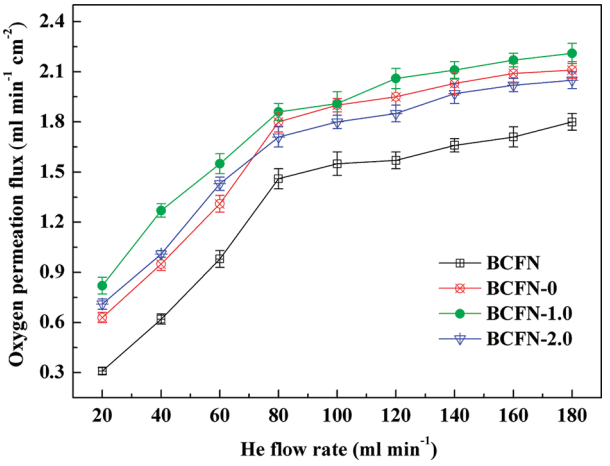

Figure 7. Effect of the He flow rate on oxygen permeation fluxes through the $GdBaCo_{2-x}Fe_xO_{5+\delta}$-coated BCFN membranes with 1.0 mm thickness. Reaction conditions: Air flow rate, 200 mL min^{-1}; temperature, 875 °C.

permeation flux changed and subsequently kept stable with the increase of the air flow rate. When the air flow rate increased from 25 to 200 mL min^{-1}, the oxygen permeation flux of the BCFN membrane increased from 0.23 to 1.55 mL min^{-1} cm^{-2}. However, when the air flow rate was higher than 200 mL min^{-1}, its influence on the membrane became negligible and the oxygen permeation flux remained about 1.55 mL min^{-1} cm^{-2}. This indicates that at the reaction temperature of 875 °C the exchange of oxygen on the air side of the membrane was the rate controlling step of oxygen permeation when the air flow rate was below 200 mL min^{-1}. Hence, the oxygen permeation flux increases with the increase of the air flow rate, whereas the oxygen permeation flux comes to a saturation level for air flow rate above 200 mL min^{-1}. This experimental finding indicates that the external diffusion of air has no influence on the oxygen permeation under the conditions. Furthermore, with the air flow rate increasing from 25 to 400 mL min^{-1}, the addition of porous catalytic materials $GdBaCo_{2-x}Fe_xO_{5+\delta}$ on the sweep side of the BCFN membrane surface can remarkably improve the oxygen

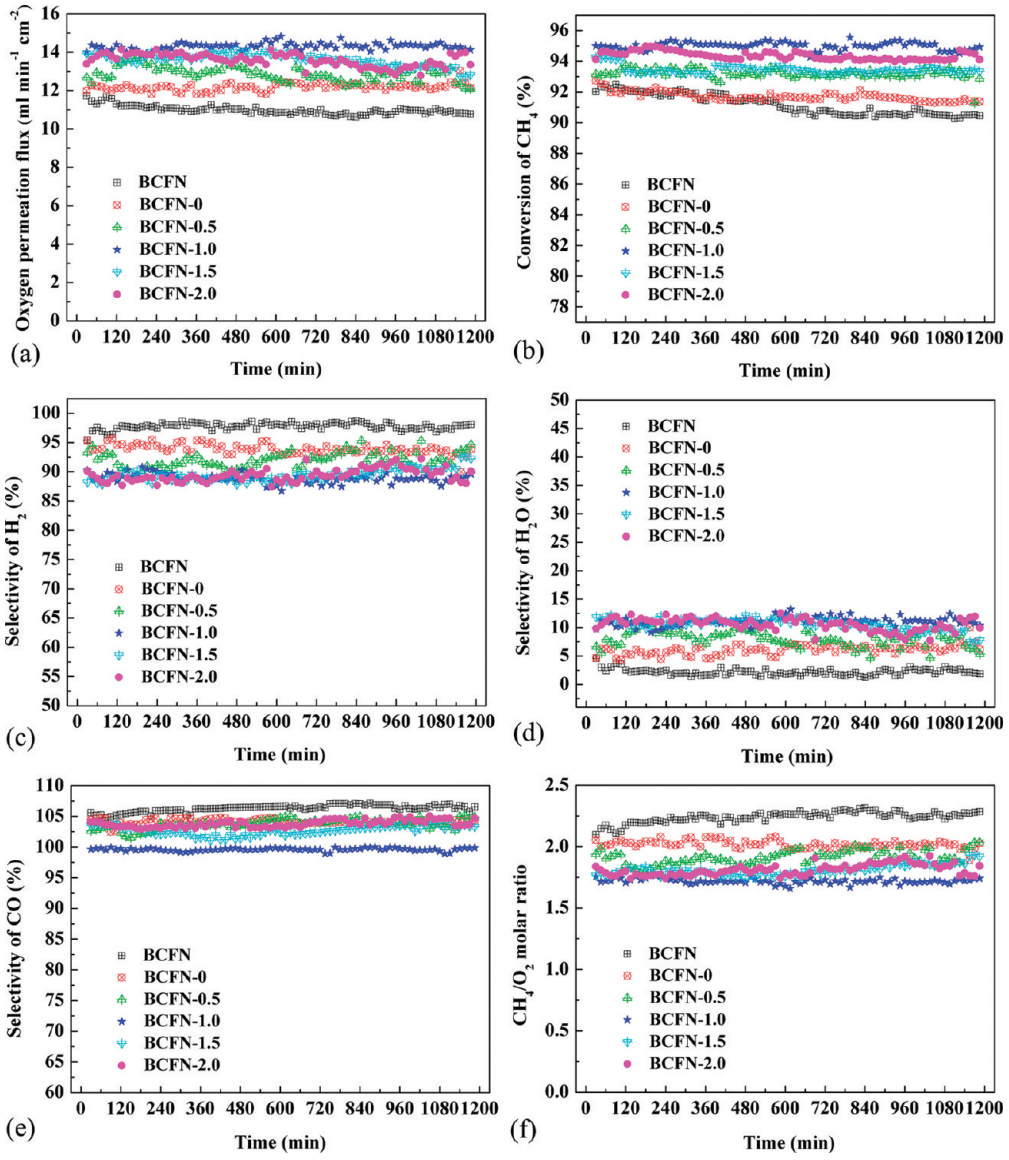

Figure 8. Effect of the coatings in the BCFN membrane reactors on (a) oxygen permeation flux; (b) CH_4 conversion; (c−e) products selectivity; (f) CH_4/O_2 molar ratio in the reforming reaction . Reaction conditions: COG flow rate, 100 mL min^{-1}; air flow rate, 200 mL min^{-1}; membrane thickness, 1.0 mm; temperature, 850 °C.

permeation flux. It is worth noting that the oxygen permeation flux through the membrane with $GdBaCoFeO_{5+\delta}$ coating layer is higher than that through the others membranes. It is probably because $GdBaCoFeO_{5+\delta}$ coating layer possesses better properties to enhance the oxygen surface exchange ability of the membrane. It has also been confirmed that the oxygen adsorption and desorption rate constants of double perovskite oxides ($LnBaCo_2O_{5+\delta}$, Ln = Gd, Pr) are much larger than that of perovskite oxides such as $Ba_{0.5}Sr_{0.5}Co_{0.8}Fe_{0.2}O_{3-\delta}$.[33,34]

The influence of different He flow rate on the oxygen permeation flux through the membranes at 875 ∘C is given in Figure 7. It is found that the oxygen permeation flux enhanced dramatically as the He flow rate is increased to 80 mL min^{-1}, whereas that returned to a slow increase with the sweep gas (He) flow rate above 80 mL min^{-1}. The sweep gas (He) flow rate has significantly influenced the oxygen partial pressure on the sweep side of the membrane.[35] According to the Wagner equation,[36] it can be concluded that the increase of the oxygen permeation flux mainly resulted from the increase of the oxygen partial gradient across the membrane. Furthermore, from Figure 7, it can be seen that the oxygen permeation flux was augmented with addition of coatings on the sweep side of the membrane. Especially, when the He flow rate was 20 mL min^{-1}, the oxygen permeation flux through BCFN-$GdBaCoFeO_{5+\delta}$ membrane was 0.82 mL min^{-1} cm^{-2}, which was 2.6 times higher than that of uncoated BCFN membrane. The porous structures can improve the ability of oxygen surface exchange, as some researchers have reported that the ability of oxygen surface exchange can be enhanced by the increase of the specific surface area (roughness) of membrane.[18,37]

3.3. Partial Oxidation of COG in the Membrane Reactors. For practical applications, the membranes not only have high oxygen permeation but also possess excellent stability in the long term operation under reducing environments. One of the most promising industrial applications of perovskite membranes is the

partial oxidation of hydrocarbons to syngas. Therefore, the catalytic partial oxidation of COG was constructed using the disk-shape BCFN membrane reactor coated with a porous layer and packed with $Ni/Ce_{0.75}Zr_{0.25}O_2/Mg_3(Al)O$ catalyst. In order to clarify the performance of the $GdBaCo_{2-x}Fe_xO_{5+\delta}$ layer to partial oxidation of CH_4 in COG, a blind experiment was also carried out in a BCFN membrane reactor without coating.

The influence of various surface-coating layers on the performance of the membrane reactor at 850 °C is shown in Figure 8. From a and b in Figure 8, it can be clearly seen that the BCFN membrane showed significant enhancement in oxygen permeation flux and CH_4 conversion during the entire reaction process by coating $GdBaCo_{2-x}Fe_xO_{5+\delta}$ layer on the permeation side. In present work, the Fe-doped $GdBaCoFeO_{5+\delta}$ sample showed the similar performance of releasing and absorbing oxygen compared with undoped sample (Figure 4). However, the results show that the BCFN membrane coated with $GdBaCoFeO_{5+\delta}$ layer achieves the best performance under COG atmosphere. It was reported that cobalt-containing layered perovskite $GdBaCo_2O_{5+\delta}$ exhibited high oxygen surface exchange coefficient and reasonable oxide ionic diffusivity.[38] Nevertheless, these cobalt-based materials often suffer from problems like poor chemical stability in CO_2, high thermal expansion coefficients, ease of evaporation, as well as high cost of cobalt element. Partial substitution of cobalt element with Fe in $GdBaCo_2O_{5+\delta}$ could potentially mitigate the disadvantages while keeping adequate electrochemical activity of cobalt-containing materials.[39,40] The average oxygen permeation flux through uncoated BCFN membrane was 10.9 mL min^{-1} cm^{-2}, whereas the values through the membrane coated using $GdBaCoFeO_{5+\delta}$ increased to 14.4 mL min^{-1} cm^{-2}, i.e., 32% higher than that of uncoated BCFN membrane. In the meantime, the corresponding conversion of CH_4 increased from 91.2 to 94.9%. Wang et al.[19] proposed that a coating layer may change the "effective" oxygen pressure imposed on the membrane surface. Therefore, the increase of the oxygen permeation flux in present experiments probably because the fast desorption ability of the coating layers can lower the "effective" oxygen pressure on the membrane surface as well as the increase of the effective surface area.

Panels c and d in Figure 8 show the influence of $GdBaCo_{2-x}Fe_xO_{5+\delta}$ surface-coating layers on the selectivity of H_2 and H_2O. It is clearly found that the selectivity of H_2 decreased, whereas that of H_2O increased with the addition of coating layer on the permeation side of the membranes. In the BCFN membrane reactor, the average selectivity of H_2 and H_2O were 97.8 and 2.2%, respectively. However, the average selectivity of H_2 lowered to 88.9%, and that of H_2O increased to 11.1% in the BCFN-1.0 membrane reactor. The diversiform tendency of the products yield was attributed to the increment of oxygen supplied by the coated membrane reacted with H_2 ($2H_2 + O_2 = 2H_2O$). The influence of the surface-coating layers on the selectivity of CO is shown in Figure 8e. It is noteworthy that the average selectivity of CO exceeded 100% in all of the membrane reactors except BCFN-1.0 (99.6%). The reason is that the oxidant was not adequate in the reaction system and the CO_2 in COG was consumed dramatically through the dry reforming reaction ($CO_2 + CH_4 = 2CO + 2H_2$). Although the oxygen permeation flux was increased, the increment of oxygen supplied by the coated membranes was not enough for the partial oxidation of methane under the conditions except BCFN-1.0. At the same time, it can be seen from Figure 8f, the minimum average CH_4/O_2 molar ratio is 1.7 in the BCFN-1.0 membrane reactor,

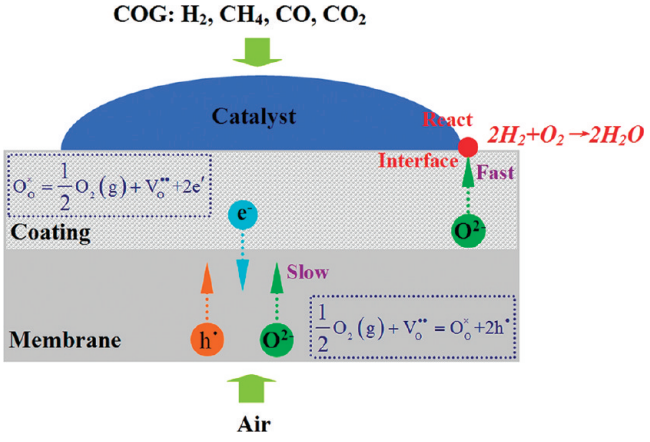

Figure 9. Schematic illustration of the oxygen permeation through coated membranes under COG atmosphere.

indicating that the oxygen was sufficient for the partial oxidation reaction ($2CH_4 + O_2 = 2CO + 4H_2$).

The possible reaction mechanism of partial oxidation of CH_4 in COG by using ceramics membrane reactor has been proposed in our previous work.[41,42] The schematic of oxygen permeation through coated membranes under COG atmosphere is outlined in Figure 9. First, the adsorbed oxygen on the air side of the membrane will be transformed into lattice oxygen ($O_O^{\times}$) by oxygen vacancies ($V_O^{\bullet\bullet}$), which will result in the generation of electron holes ($h^{\bullet}$). Then the lattice oxygen withdraws two electrons from the membrane and dissociates into oxygen ions. Driven by the oxygen partial pressure gradient across the membrane, the oxygen ions diffuse across the membrane bulk to the membrane surface on the oxygen-poor side, where they recombine with electron holes to form lattice oxygen. Finally, the lattice oxygen will be lost on the reduction surface of the membrane, which will result in the generation of molecular oxygen, oxygen vacancies and electrons. The generated electrons are captured by the electron holes, which result in the whole of the membrane is electrically neutral. On the permeation side of the membrane, if the coating layer has a faster oxygen desorption rate than the membrane material, oxygen ions can dissipate in the coating layer and a lower oxygen pressure will be formed on the surface of the membrane. This oxygen pressure can enhance the oxygen permeation flux through the membrane. In fact, from the results of TG experiments, it is reasonable to consider that the oxygen desorption rate and the amount of oxygen released of the $GdBaCoFeO_{5+\delta}$ surface-coating layer are much larger than that of BCFN.

4. CONCLUSIONS

Hydrogen production from COG by partial oxidation of methane was investigated by using a BCFN membrane reactor combined with $GdBaCo_{2-x}Fe_xO_{5+\delta}$ surface-coating layers. The results of experimental tests indicated that the surface-exchange kinetics is one of the rate determining steps for oxygen permeation through the membrane. The oxygen permeation fluxes for the BCFN membranes surface-modified by the layers on the permeation side were 20−44% higher than that for uncoated BCFN membrane under the He atmosphere at 750 °C. The increases of the reaction temperature, air flow rate and He sweep gas flow rate were beneficial to improve the oxygen permeation flux.

The maximum oxygen permeation flux reached 14.4 mL min^{-1} cm^{-2} in the $GdBaCoFeO_{5+\delta}$ coated BCFN membrane reactor at 850 °C, and 94.9% CH_4 conversion, 88.9% H_2 selectivity, 99.6% CO selectivity have been achieved. The $GdBaCo_{2-x}Fe_xO_{5+\delta}$ coating materials can sharply improve the oxygen permeation flux under COG atmosphere, which will be promising surface modification materials for hydrogen production from COG by catalytic partial oxidation reforming of methane in a BCFN membrane reactor.

AUTHOR INFORMATION

Corresponding Author

*Telephone/Fax: +86-21-56338244. E-mail: hwcheng@shu.edu.cn (H.W.C.); luxg@shu.edu.cn (X.G.L.).

ACKNOWLEDGMENT

The financial supports received from the National High Technology Research and Development Program of China (2006AA11A189), the National Natural Science Foundation of China (51004069), and China Postdoctoral Science Foundation (201104254) are greatly appreciated.

REFERENCES

(1) Weinert, J. X.; Liu, S. J.; Ogden, J. M.; Ma, J. X. *Int. J. Hydrogen Energy* **2007**, *32*, 4089–4100.
(2) Cheekatamarla, P. K.; Finnerty, C. M.; Cai, J. *Int. J. Hydrogen Energy* **2008**, *33*, 1853–1858.
(3) Li, J. C.; Yu, H.; Yang, G. X.; Peng, F.; Xie, D. L.; Wang, H. J.; Yang, J. *Energy Fuels* **2011**, *25*, 2643–2650.
(4) Brunetti, A.; Barbieri, G.; Drioli, E. *Energy Fuels* **2009**, *23*, 5073–5076.
(5) Dufour, J.; Serrano, D. P.; Galvez, J. L.; Moreno, J.; Gonzalez, A. *Energy Fuels* **2011**, *25*, 2194–2202.
(6) Chun, Y. N.; Song, H. W.; Kim, S. C.; Lim, M. S. *Energy Fuels* **2008**, *22*, 123–127.
(7) Joseck, F.; Wang, M.; Wu, Y. *Int. J. Hydrogen Energy* **2008**, *33*, 1445–1454.
(8) Shen, J.; Wang, Z. Z.; Yang, H. W.; Yao, R. S. *Energy Fuels* **2007**, *21*, 3588–3592.
(9) Zhang, Y. W.; Li, Q.; Shen, P. J.; Liu, Y.; Yang, Z. B.; Ding, W. Z.; Lu, X. G. *Int. J. Hydrogen Energy* **2008**, *33*, 3311–3319.
(10) Yang, Z. B.; Ding, W. Z.; Zhang, Y. Y.; Lu, X. G.; Zhang, Y. W.; Shen, P. J. *Int. J. Hydrogen Energy* **2010**, *35*, 6239–6247.
(11) Cheng, H. W.; Zhang, Y. W.; Lu, X. G.; Ding, W. Z.; Li, Q. *Energy Fuels* **2009**, *23*, 414–421.
(12) Cheng, H. W.; Lu, X. G.; Zhang, Y. W.; Ding, W. Z. *Energy Fuels* **2009**, *23*, 3119–3125.
(13) Cheng, H. W.; Lu, X. G.; Liu, X.; Zhang, Y. W.; Ding, W. Z. *J. Nat. Gas Chem.* **2009**, *18*, 467–473.
(14) Zhan, M. C.; Wang, W. D.; Tian, T. F.; Chen, C. S. *Energy Fuels* **2010**, *24*, 764–771.
(15) Park, C. Y.; Lee, T. H.; Dorris, S. E.; Balachandran, U. *Int. J. Hydrogen Energy* **2010**, *35*, 4103–4110.
(16) Waindich, A.; Mobius, A.; Muller, M. *J. Membr. Sci.* **2009**, *337*, 182–187.
(17) Cheng, H. W.; Lu, X. G.; Hu, D. H.; Zhang, Y. W.; Ding, W. Z.; Zhao, H. L. *Int. J. Hydrogen Energy* **2011**, *36*, 528–538.
(18) Kida, T.; Ninomiya, S.; Watanabe, K.; Yamazoe, N.; Shimanoe, K. *ACS Appl. Mater. Interfaces* **2010**, *2*, 2849–2853.
(19) Wang, Y. F.; Hao, H. S.; Jia, J. F.; Yang, D. L.; Hu, X. *J. Eur. Ceram. Soc.* **2008**, *28*, 3125–3130.
(20) Zhu, X. F.; Cong, Y.; Yang, W. S. *J. Membr. Sci.* **2006**, *283*, 38–44.
(21) Figueiredo, F. M.; Kharton, V. V.; Viskup, A. P.; Frade, J. R. *J. Membr. Sci.* **2004**, *236*, 73–80.
(22) Leo, A.; Liu, S. M.; Diniz da Costa, J. C. *J. Membr. Sci.* **2009**, *340*, 148–153.
(23) Chen, Z. H.; Shao, Z. P.; Ran, R.; Zhou, W.; Zeng, P. Y.; Liu, S. M. *J. Membr. Sci.* **2007**, *300*, 182–190.
(24) Zhang, K.; Ge, L.; Ran, R.; Shao, Z. P.; Liu, S. M. *Acta Mater.* **2008**, *56*, 4876–4889.
(25) Kim, J. H.; Mogni, L.; Prado, F.; Caneiro, A.; Alonso, J. A.; Manthiram, A. *J. Electrochem. Soc.* **2009**, *156*, B1376–B1382.
(26) Kim, G.; Wang, S.; Jacobson, A. J.; Yuan, Z.; Donner, W.; Chen, C. L.; Reimus, L.; Brodersen, P.; Mims, C. A. *Appl. Phys. Lett.* **2006**, *88* (024103), 1–3.
(27) Wei, B.; Lu, Z.; Jia, D. C.; Huang, X. Q.; Zhang, Y. H.; Su, W. H. *Int. J. Hydrogen Energy* **2010**, *35*, 3775–3782.
(28) Lee, S. J.; Kim, D. S.; Muralidharan, P.; Jo, S. H.; Kim, D. K. *J. Power Sources* **2011**, *196*, 3095–3098.
(29) Kim, Y. N.; Kim, J. H.; Manthiram, A. *J. Power Sources* **2010**, *195*, 6411–6419.
(30) Xue, J. F.; Shen, Y.; He, T. M. *J. Power Sources* **2011**, *196*, 3729–3735.
(31) Teraoka, Y.; Honbe, Y.; Ishii, J.; Furukawa, H.; Moriguchi, I. *Solid State Ionics* **2002**, *152−153*, 681–687.
(32) Watanabe, K.; Yuasa, M.; Kida, T.; Shimanoe, K.; Teraoka, Y.; Yamazoe, N. *Solid State Ionics* **2008**, *179*, 1377–1381.
(33) Hu, J.; Hao, H. S.; Chen, C. p.; Yang, D. L.; Hu, X. *J. Membr. Sci.* **2006**, *280*, 809–814.
(34) Hao, H. S.; Zheng, L.; Wang, Y. F.; Liu, S. J.; Hu, X. *J. Rare Earths* **2007**, *25*, 275–281.
(35) Akin, F. T.; Lin, J. Y. S. *J. Membr. Sci.* **2004**, *231*, 133–146.
(36) Xu, S. J.; Thomson, W. J. *Chem. Eng. Sci.* **1999**, *54*, 3839–3850.
(37) Kusaba, H.; Shibata, Y.; Sasaki, K.; Teraoka, Y. *Solid State Ionics* **2006**, *177*, 2249–2253.
(38) Tarancon, A.; Skinner, S.; Chater, R.; Ramirez, F.; Kilner, J. *J. Mater. Chem.* **2007**, *17*, 3175–3181.
(39) Ding, H. P.; Lin, B.; Liu, X. Q.; Meng, G. Y. *Electrochem. Commun.* **2008**, *10*, 1388–1391.
(40) Ding, H. P.; Xue, X. J. *Int. J. Hydrogen Energy* **2010**, *35*, 4311–4315.
(41) Shen, P. J.; Ding, W. Z.; Zhou, Y. D.; Huang, S. Q. *Appl. Surf. Sci.* **2010**, *256*, 5094–5101.
(42) Zhang, Y. W.; Liu, J.; Ding, W. Z.; Lu, X. G. *Fuel* **2011**, *90*, 324–330.